BMP signaling is enhanced intracellularly by FHL3 controlling WNT-dependent spatiotemporal emergence of the neural crest

Mansour Alkobtawi, Patrick Pla, Anne Monsoro-Burq

Intracellular enhancement of BMP signaling by LIM-domain protein FHL3 controls spatiotemporal emergence of the neural crest driven by WNT signaling.

Mansour Alkobtawi[1,2], Patrick Pla[1,2§] and Anne H. Monsoro-Burq[1,2,3*].

[1,] Université Paris-Saclay, CNRS UMR 3347, INSERM U1021,F-91405 Orsay, France.

[2,] Institut Curie Research Division, PSL Research University, rue Henri Becquerel, F-91405, Orsay, France.

[3,] Institut Universitaire de France, F-75005, Paris.

[§]co-supervisor

*Author for correspondance and Lead Contact: Anne H. Monsoro-Burq; anne-helene.monsoro-burq@curie.fr

Summary

The spatiotemporal coordination of multiple morphogens is essential for embryonic patterning yet poorly understood. During neural crest (NC) formation dynamic BMP, FGF and WNT signals cooperate by acting on mesoderm and ectoderm. Here we show that Fhl3, a scaffold LIM domain protein, modulates BMP gradient interpretation during NC induction. During gastrulation low BMP signaling neuralizes the neural border (NB) ectoderm while Fhl3 enhances Smad1 intracellular response in underlying paraxial mesoderm triggering the high WNT8 signals needed to pattern the NB. During neurulation *fhl3* activation in NC ectoderm promotes simultaneous high BMP and BMP-dependent WNT activity required for specification. Mechanistically, Fhl3 interacts with Smad1 and promotes Smad1 binding to *wnt8* promoter in a BMP-dependent manner. Consequently, differential Fhl3 expression in adjacent cells ensure a finely tuned coordination of BMP and WNT signaling at several stages of NC development, starting by positioning the NC-inducing mesoderm center under competent NB ectoderm.

Keywords: four and a half LIM domain protein 3; neural crest gene regulatory network

Introduction

A strict spatiotemporal control of bone morphogenetic proteins (BMP) activity is crucial for both mesoderm and ectoderm patterning (Bier and De Robertis, 2015). Intricate additional morphogen gradients further refine germ layer subdivision. Neural crest (NC) development is an ideal paradigm to model multiple tightly controlled inputs in patterning. The NC is induced from the neural border ectoderm (NB), precisely located lateral to the neural plate (NP) of early gastrulas in response to BMPs, WNTs and fibroblast growth factors (FGFs) diffusing from the ectoderm and/or from the underlying mesoderm (De Crozé et al., 2011; Garnett et al., 2012). Later on during neurulation, additional BMP and WNT planar ectodermal signals control further NC development (Pla and Monsoro-Burq, 2018). While each pathway has been studied separately in NC formation, how these signals are coordinated and how adjacent cells, submitted to similar extracellular inputs, may interpret differentially this complex information remains poorly understood.

A fine-tuned dynamic modulation of BMP signaling positions the NC and promotes sequential steps of NC formation (Kuriyama et al., 2006; Piacentino and Bronner, 2018; Wu et al., 2011). Specifically, ventral BMPs diffuse towards dorsal tissues, while dorsal BMP antagonists diffuse ventrally along Brachet's cleft, the space separating mesoderm from ectoderm (Plouhinec et al., 2013). This creates a net gradient of extracellular BMP activity which patterns ectoderm and mesoderm simultaneously. Consequently the paraxial and intermediate mesoderm and the overlying NB ectoderm receive similar moderate BMP signals at gastrula stage (Harland and Gerhart, 1997). In the gastrula ectoderm, low BMP signaling allows NP induction, intermediate levels pattern NB and NC, while high BMP activity promotes non-neural ectoderm fates (De Robertis and Kuroda, 2004; LaBonne and Bronner-Fraser, 1998). Later during neurulation however, enhanced BMP signaling in the neural folds promote further NC development (Litsiou et al., 2005; Steventon et al., 2012; Wu et al., 2011).

BMP signaling molecular cascade involves BMP ligand binding to membrane receptors triggering Smad1/5/8 phosphorylation and dimerization. Smad1/5/8 complex with

Smad4, translocate into the nucleus and regulate target genes in a BMP dose-dependent manner (Massagué et al., 2005). A first major question during NC induction is whether the moderate levels of BMP signaling are interpreted similarly by the mesoderm and the overlying ectoderm. Moreover, intermediate levels of BMP activity are not sufficient for a robust NB induction: WNT and FGF signals from the mesoderm cooperate with BMPs to activate the NB/NC gene regulatory network (GRN) in the ectoderm: when NB is specified in frog gastrulas, the underlying mesoderm expresses FGF and WNT ligands diffusing towards the overlying ectoderm, all essential for NB-NC activation (Chang and Hemmati Brivanlou, 1998; Garnett et al., 2012; Monsoro-Burq et al., 2003; Saint-Jeannet et al., 1997). BMP signaling also triggers *wnt8* expression in the mesoderm; in turn Wnt8 patterns the paraxial mesoderm (Hoppler and Moon, 1998). Importantly BMP and WNT relative signaling levels are dynamically orchestrated during gastrulation and neurulation: low BMP/high WNT signals induce NB, followed by high BMP/high WNT to induce NC (Steventon et al., 2009). Thus, a second major question is how these various signals are modulated and coordinated with the initial BMP gradient, either in the responding ectoderm or mesoderm (spatial coordination), or during gastrulation and neurulation (temporal coordination).

We found that the four-and-a-half LIM domain scaffold protein Fhl3 is critical for the intracellular interpretation of BMP signals during frog NB and NC development. FHL proteins broadly regulate cell proliferation, differentiation and apoptosis (Bach, 2000). Fhl3 modulates cell signaling and gene transcription in adult and cancer tissues by protein-protein interactions but its developmental function is unknown (Kadrmas and Beckerle, 2004). Fhl3 interacts with Smad2/3/4 and modulates TGFβ signaling in cancer, while Fhl3 promotes myoblast proliferation *in vitro* by binding MyoD and Sox15 (Ding et al., 2009; Han et al., 2018; Meeson et al., 2007). Here, we find that Fhl3 is dynamically and differentially expressed in mesoderm and ectoderm during gastrulation and neurulation. Fhl3 enhances paraxial mesoderm response to BMPs and promotes WNT signaling towards the prospective NB ectoderm. Later on, Fhl3 activity promotes BMP and WNT signals in premigratory NC itself. We find that Fhl3 binds Smad1 and promotes its activity. Last, we show how by their

differential expression of *fhl3*, apposed ectoderm and mesoderm exhibit different levels of response to the intermediate BMP signals during gastrulation. Our results identify Fhl3 as a key modulator of cell response to morphogens and show how this impacts the activation of several steps of the NC-GRN.

Results

Fhl3, first expressed in gastrulating mesoderm and later in NC cells, is essential for NC development

Fhl3 developmental expression was compared to the patterns of ectoderm regional markers in *Xenopus laevis* embryos: *pax3, sox2* and *snai2* for NB, NP and NC respectively. At early gastrula stage, *fhl3* labeled the involuting mesoderm (dorsal marginal zone/DMZ and dorsal-lateral marginal zone/DLMZ). *Fhl3* remained expressed in the axial (notochord) and paraxial/intermediate mesoderm until tailbud stage (Figures 1A, S1A-F). *Fhl3* expression then labeled NB ectoderm at late gastrula stage (Figure S1B). In neurulas *fhl3* was seen in all premigratory NC cells, starting with the hyoid stream (Figure 1A, S1D). At tailbud stage *fhl3* was found in the migratory NCCs with stronger levels in the hyoid stream (Figure S1D). *Fhl3* was later observed in branchial arches, notochord and somites (Figure S1D-F). In this study, we focused on Fhl3 function in the two key tissues involved in NC induction: the dorsal mesoderm inducing the overlying NB in the ectoderm at gastrula stage, and the NB and premigratory NC in neurulas.

To assess its developmental function *in vivo*, we depleted Fhl3 unilaterally using a translation-blocking morpholino (MO), a splice-blocking MO or CRISPR/cas9-mediated *fhl3* mutation (Figure 1B-F, S2A-F). The phenotype rescue by human FHL3 mRNA assessed MO specificity and indicated that FHL3 function was evolutionarily conserved (Figure S2C). Upon Fhl3 knockdown (KD, Figure 1B-D, S2D-F), NB markers *tfap2a*, *pax3* and *msx1* were severely downregulated while others (e.g. *zic1*) were unchanged or upregulated, as was the NP marker *sox2*. This showed that *fhl3* morphant NB ectoderm formed (*zic1*-positive) but

100 was mispatterned. Expression of *tbxt* (*xbra,* pan-mesoderm) and *myod* (paraxial mesoderm)
101 was unaffected indicating globally normal mesoderm formation. Thus, Fhl3 KD did not affect
102 the initial formation of dorsal mesoderm and ectoderm during gastrulation but was essential
103 for NB early patterning. At neurula stage Fhl3 KD downregulated all premigratory NC
104 markers (*snai2, foxd3, twist1*, *sox10*, Figure 1C). Instead, the NP was enlarged (*sox2*) at the
105 expense of NC (*snai2* or *twist1*) and of non-neural ectoderm (*epidermal keratin epK).*
106 Transverse sections show the lateral expansion of the neural tissue (*sox2*) and the lateral
107 shift of the reduced *snai2/twist1* territories while the underlying mesoderm was normal
108 (Figure 1D, S2F). At tailbud stage, migration of Fhl3 morphant cranial NC cells was markedly
109 reduced (*twist1*, Figure 1E) while other tissues (e.g. eye) were unaffected. This resulted in
110 severe craniofacial skeleton defects (Figure 1F): the *trabeculae cranii* derived from the
111 mandibular and hyoid arches were missing and branchial arches were atrophied. Together,
112 these results showed that Fhl3 was necessary for NB and NC induction by causing strong
113 early developmental defects.

114 Last, we injected *fhl3* mRNA unilaterally to test Fhl3 gain-of-function (GOF) on NB
115 and NP formation compared to the uninjected contralateral side. Both at late gastrula and
116 neurula stages, increased and ectopic expression of *Fhl3* disrupted NB/NP patterning. NP
117 size was reduced and *sox2* expression levels were decreased. In contrast, the NB was
118 strongly expanded (*pax3,* Figure 1G) towards both the midline and the lateral ectoderm. This
119 suggested that an ectopic NB state was imposed on NP progenitors, while NP was reduced.
120 However, this ectopic NB was incompletely specified, lacking expansion of other NB markers
121 (*tfap2a,* not shown). Those disruptions resulted in decreased *snai2 a* usual consequence of
122 perturbing the NC-GRN equilibrium. This NP/NC reduction phenotype phenocopied an
123 increased BMP signaling obtained by injecting constitutively active (ca) BMP receptor mRNA
124 unilaterally (Figure 1G).

125 Altogether expression, KD and GOF results suggested that Fhl3 was essential for
126 NB/NC formation, potentially acting in mesoderm or ectoderm at different developmental
127 stages.

Fhl3 controls BMP signaling in the paraxial mesoderm

The pattern alterations observed above could result from abnormal signaling in the early NB/NC-GRN. Lower BMP signaling after Fhl3 depletion could expand the NP and shift/reduce the NB laterally while higher BMP signaling after Fhl3 GOF would have the converse phenotype. During NB induction, low BMP signaling triggers *zic1* expression, while high WNT signaling activates *tfap2a*, *pax3,* and *msx1* (De Crozé et al., 2011; Mizuseki et al., 1998). Thus, low BMP and low WNT signals could result in the pattern deregulations observed in Fhl3-depleted embryos. We found that *Fhl3* mesodermal expression increased in the DLMZ at late gastrula stages, i.e. when NB ectoderm was induced, compared to early gastrula stage (Figure S3A). We then measured the response to BMP signaling in the mesoderm after co-injecting a BMP reporter (Kusanagi et al., 2000) with *fhl3* MO and dissecting the DLMZ out of early gastrulas. Response was significantly reduced in *fhl3* morphant DLMZ compared to controls (Figure 2A-B). Thirdly we used tissue recombination to test how the paraxial mesoderm induced NB/NC after Fhl3 KD, by apposing a gastrula-stage DLMZ to a piece of late blastula-stage animal cap ectoderm (AC, Bonstein et al., 1998; Figure 2C). Compared to control DLMZ, *fhl3* morphant DLMZ failed to activate NB and NC markers (*pax3*, *snai2, sox10*). Last, we tested if the altered BMP signaling observed in the morphant mesoderm caused its lack of inducing activity by a phenotype rescue, i.e. by co-injecting *fhl3* MO with caSmad1 or of caBMPR1. The co-injected DLMZ activated *pax3* and *snai2* expression better than morphant DLMZ but lower than uninjected controls (Figure 2C). These results showed that Fhl3 function in the paraxial mesoderm was critical for NC induction in the ectoderm, at least partly by promoting BMP signaling.

Fhl3 controls vertical Wnt8 signaling acting between paraxial mesoderm and ectoderm during NC induction

WNTs and FGFs from the paraxial mesoderm are crucial for inducing the NC. We quantified the expression of *dusp5* (FGF-responsive gene) and *axin2* (canonical WNT signaling readout) in mesoderm-ectoderm recombinants (Figure 2D). *Axin2* expression was reduced in the *fhl3* morphant recombinants but not *dusp5* levels, suggesting altered WNT activity and normal FGF function. To confirm that Fhl3 KD, when restricted to the mesoderm, resulted in altered canonical WNT signaling specifically in the ectoderm, we injected the WNT/β-catenin signaling reporter into the ectoderm only, and juxtaposed it to either uninjected or *fhl3* morphant DLMZ. Compared to controls, the ectoderm combined to morphant mesoderm showed a strongly decreased response to WNT signaling (Figure 2E) showing that the levels of WNT activity in the ectoderm depended on Fhl3 function specifically in the mesoderm. We tested if the decreased WNT signaling observed in ectoderm after Fhl3 KD in the mesoderm explained the lack of NC induction with a phenotype rescue using either an inducible form of caTCF3 or *wnt8* GOF, injected in the ectoderm only (Figure 2F). When uninduced ectoderm was juxtaposed to Fhl3-depleted DLMZ, *pax3* and *snai2* expression levels were as low as in uninjected ectoderm above. In contrast induction of caTCF3 or Wnt8 GOF in the ectoderm fully restored *pax3* and *snai2* levels. Together, these results demonstrated that Fhl3 early function in the paraxial mesoderm was critical for its ability to activate WNT signaling at levels required for NC induction in the ectoderm.

During neurulation, Fhl3 is necessary for NC induction by NB specifiers and controls both BMP and WNT signaling levels in the ectoderm

Interestingly, neurula-stage *fhl3* ectodermal expression partly overlapped with *pax3* pattern consistent with the identification of *fhl3* as a putative target of Pax3 (Bae et al., 2014). Indeed, unilateral Pax3 GOF or KD *in vivo* modestly expanded or fully eliminated *fhl3* expression respectively (Figure S4A). This replaced *fhl3* as a new member of the NC-GRN activated in the ectoderm, downstream of NB specification.

We then directly measured *fhl3* expression in ectoderm (Figure S4B-C). In AC grown *in vitro* forming non-neural ectoderm, the levels of *fhl3* increased at neurula stage. In ectoderm-specific transcriptomes (Plouhinec et al., 2017) we found high *fhl3* expression in the ventral non-neural ectoderm, intermediate levels in NB ectoderm and low levels in the NP. Last, Fhl3 depletion promoted neural induction (*sox2)* in AC ectoderm (Figure S4D) suggesting that Fhl3 globally modulated tissue response to BMP signaling in the ectoderm too.

We have then used a direct NC induction assay (iNC, Figure 3A) in order to separate the roles of *fhl3* within the ectoderm from its mesodermal functions. Calibrated GOF of Pax3 and Zic1 triggers the NC-GRN in AC ectoderm (Milet et al., 2013). Compared to control iNC, co-injecting *fhl3* MO prevented NC activation (*snai2, sox10*) suggesting that Fhl3 was also required for premigratory NC specification downstream of NB regulators (Figure 3B). Moreover, *pax3* expression was also decreased suggesting that Pax3 positive autoregulatory loop was also defective (Plouhinec et al., 2014).

Next, we tested if Fhl3 depletion in iNC affected BMP and WNT signaling as observed in the mesoderm. After *fhl3* KD, BMP and WNT signaling reporters activity was severely reduced compared control iNC while co-injection of either caSmad1 or *wnt8* in *fhl3* morphant iNC rescued *snai2* and *pax3* expression (Figure 3C-D). As in the mesoderm, caSmad1 rescued *snai2* with lower efficiency than Wnt8. Thus, at neurula-stage steps the NC-GRN, Fhl3 is essential for NC specification by promoting both BMP and WNT signaling in the prospective NC.

The striking parallel observed between BMP activity and WNT signaling in all the results above, either in the mesoderm or in the ectoderm, led us to hypothesize that Fhl3 participated to the known transcriptional cross-talk between the two signaling pathways (Hoppler et al., 1998). We tested this potential interaction directly by Fhl3 KD either in the mesoderm or in the iNC combined to BMP activation. Either caSmad1 GOF or caBMPR GOF restored *wnt8* and *axin2* expression in morphant DLMZ recombined to control ectoderm and in morphant iNC (Figure 3E). Here, the rescue was efficiently achieved with both caSmad1

and caBMPR suggesting that the mechanisms controlling *wnt8* expression after Fhl3 KD were more direct than those controlling *snai2* (Figure 2C, 3D). This also suggested that in both assays Fhl3 might enhance Smad1 activity resulting in up-regulated *wnt8* expression. We thus hypothesized that Fhl3 potentiated BMP signaling in a non-essential manner, since decreased Fhl3 activity was compensated by increased BMP signaling, indicating that the BMP molecular cascade remained functional in the absence of Fhl3.

Fhl3 interacts with Smad1 and promotes its binding to *wnt8* promoter

We thus examined *wnt8* expression *in vivo* after Fhl3 KD: Fhl3 morphant mesoderm displayed diminished expression of *wnt8* and WNT-responsive gene *myf5* compared to the uninjected control side (Figures 4A, S2D). Although Smad1/5/8 phosphorylation was strongly decreased in DLMZ, we did not find defective BMPR activity or phospho-Smad stability (Figure S3). We thus hypothesized that Fhl3 may potentiate Smad1 nuclear shuttling, binding or activity on target sequences by protein-protein interactions. As BMP signals regulate mesodermal *wnt8* transcription (Hoopler et al., 1998), we searched for and found two putative Smad-binding/BMP-responsive (BRE) elements upstream of *wnt8* transcriptional start (BS1 at position -1571; BS2 at position -674). To validate BS1 we used EMSA with a wild-type or a mutated BS1 primer (mut-BS1). Cell nuclear extracts with GFP shifted BS1 primer indicating endogenous Smad1 binding. Both Smad1 and Fhl3 transfections enhanced BS1 shifting, which was lost with mut-BS1 (Figure 4A). This validated the importance of the TAGAC motif in BS1 for Smad1 binding. Using ChIP-qPCR at late gastrula stage (Figure 4A-B), we further tested if Smad1 and Fhl3 were found in protein complexes bound to BS1 and BS2 *in vivo* and if this was regulated by BMP signaling. *Ventx1.1* gene BRE was a positive control (Lee et al., 2011). BS1, BS2 and *ventx1.1* BRE were all found strongly enriched in the Fhl3-bound chromatin compared to background. This enrichment was no longer detected after co-injection of *noggin* showing that Fhl3 specifically bound *wnt8* promoter when BMP signaling was active. We next validated Smad1 occupancy at BS1, BS2 and *ventx1.1* BRE sites. Furthermore, the efficiency of Smad1 binding on BS1, BS2 and *ventx1.1* BRE *in vivo*

was reduced after Fhl3 KD and increased after Fhl3 GOF (Figure 4B). Altogether, these experiments identify an Fhl3-dependent binding of Smad1 on *wnt8* promoter. Fhl3 binding to the same chromatin regions suggests that Smad1 and Fhl3 are likely engaged together in a transcriptional complex regulating *wnt8* expression. The response of *ventx1.1* BRE showed a similar dependency to Fhl3 levels, suggesting a broad role of Fhl3 in the regulation of BMP-responsive genes in embryos.

We then tested if Fhl3 could affect Smad1 nuclear shuttling. First, at high BMP levels, we found Fhl3 enriched in the nucleus of ectoderm cells (AC) and of HEK293 cells while Fhl3 was mainly in the cytoplasm of AC injected with *noggin* (Figure 4C, S5A). In HEK293 cells, Fhl3 transfection increased Smad1 nuclear localization suggesting enhanced shuttling of Smad1 in presence of Fhl3 (Figure S5A). We further tested if FHL3 and Smads interacted directly by co-immunoprecipitation (IP) using HEK293 cells or whole embryo extracts, but detected only a modest enrichment of FHL3 after IP by FLAG-Smad1 or of Smad1 after IP with HA-tagged FHL3 (Figures 4D, S5B). To overcome IP limitations to detect transient interactions or interactions between proteins in a larger complex, we then used a two-hybrid assay tuned for mammalian cells, which robustly detects the transcriptional outcome a given protein-protein interactions occurring *in cellulo* prior to cell lysis. We found that Fhl3 robustly interacted with Smad1 and Smad4, Smad2 being a positive control (Figure 4E, Han et al., 2018) indicating that Fhl3 and Smad1/4 belonged to the same protein complex *in vivo*.

Altogether, our results supported a model where, upon BMP signaling, Fhl3 interacted with the Smad1/4 complex, shuttled into the nucleus and enhanced Smad1 binding to its target genes including *wnt8*.

At intermediate BMP levels, tissue-specific Fhl3 expression selectively coordinates NB ectoderm neuralization with mesoderm higher response to BMPs

To understand if Fhl3 modulated generic BMP signaling in a homogeneous tissue grown in isolation, we tested Fhl3 effects on BMP response in AC injected with the standard BMP-reporter (Figure 5A). For Fhl3 GOF assay, we lowered the high endogenous BMP

levels found in AC with a low dose of *noggin*. Co-injection of increasing doses of *fhl3* mRNA resulted in a graded increase in BMP response. Conversely, increasing doses of Fhl3 MO caused a dose-dependent decrease of BMP response in AC. As AC were grown *in vitro* without growth factors, this ensured the lack of interfering regulation. These results showed that, at a given level of BMP signaling, Fhl3 levels influenced the response of a generic BMP-reporter in a dose-dependent manner.

Last, we sought to understand the significance of Fhl3 action *in vivo*, in the context of the tissue response to the ventral-to-dorsal BMP gradient, and between the mesoderm and ectoderm germ layers during gastrulation. The results above collectively suggest that, when subjected to the same levels of extracellular BMP signals, cells expressing Fhl3 would respond to BMPs higher than cells without Fhl3. We thus directly measured tissue response to BMP in wt and Fhl3 morphant gastrula-stage mesoderm positioned dorsally (submitted to very low BMP levels), dorsal-laterally (intermediate BMP levels) and ventrally (high BMP levels) (Figure 5B) by dissecting DMZ, DLMZ and VMZ injected with BMP-reporter alone or together with Fhl3 MO. All explants were homogeneous fragments of embryonic mesoderm without any contact with another tissue that might modulate their response to BMP. Thus, this experiment directly measured BMP response in the mesoderm along the endogenous BMP gradient. We find that wt ventral and dorsal-lateral mesoderm respond similarly to BMPs while dorsal mesoderm had a low response (set to basal level). Upon Fhl3 depletion, response of DMZ and VMZ were unchanged, while DLMZ response was abolished. This experiment uncovered three points. First, as expected upon the action of BMP antagonists, the DMZ responded weakly to BMP signaling despite its expression of Fhl3, confirming that Fhl3 action was dependent on BMP signals. Secondly, in the ventral mesoderm, producing high BMP levels, a strong BMP response is achieved with or without Fhl3. In contrast, Fhl3 action had a strong impact on the response of intermediate mesoderm: the DLMZ response to intermediate BMP levels was as strong as one observed ventrally and not an "intermediate level" response as previously proposed, and this resulted from Fhl3 activity.

Lastly, we hypothesized that at paraxial levels of gastrula-stage embryos, i.e. at the same position along the dorsal-ventral (DV) BMP gradient, the Fhl3-positive DLMZ would respond stronger to the moderate BMP levels than the Fhl3-negative ectoderm. We dissected out separately the gastrulating mesoderm or the adjacent ectoderm, both coming from the same DV position, either injected with BMP-reporter alone or together with Fhl3 MO (Figure 5C). As predicted, the mesoderm (DLMZ) response was higher and Fhl3-dependent while the response by the prospective NB ectoderm (DL-EC) was low (equivalent to the response by the axial DMZ) and unchanged upon Fhl3 depletion, consistent with lack of expression in the ectoderm at gastrula stage. These data thus showed that at paraxial position, Fhl3 controlled the response to BMPs in a tissue-specific manner, such that the mesoderm responded as strongly as ventral mesoderm, while in the ectoderm, the low response was compatible with neuralization of the NB. This differential tissue response during gastrulation, dependent upon Fhl3, thus controlled the relative positioning of the NC-inducing paraxial mesoderm (secreting WNTs) underneath the responsive NB ectoderm, thereby triggering NC formation (Figure 5D).

Discussion.

Fhl3 is a novel enhancer of BMP signaling which controls several steps in the NC-GRN in vivo.

Early patterning and later organogenesis are the result of a remarkably orchestrated suite of signaling and inductive interactions. However, how each germ layer or subsets of cells in each tissue respond to the broad morphogen gradients set up during early embryogenesis remains incompletely understood. Moreover, the parameters controlling the relative dynamics of multiple signals are still largely unknown. For example, the relative levels of BMP and Wnt signaling needed for the different steps of the NC-GRN are highly dynamic (Steventon et al., 2009) but how these signaling modulations are obtained locally, and how they impact the mesoderm-ectoderm interactions and further regulations in NC remains unexplored. Here, we used tissue-specific gene manipulations, either in isolation or

combined to other embryonic tissue recombination at several stages of development to disentangle the sequence of events involving the scaffold protein Fhl3 in early NB/NC induction.

Fhl3 is activated in the involuting dorsal mesoderm during gastrulation and in the prospective NC ectoderm during neurulation. Fhl3 depletion or GOF alters the NC-GRN but not initial mesoderm patterning. Fhl3 controls the NC-inducing properties of the paraxial mesoderm at gastrula stages and participates to ectoderm patterning in neurulas by enhancing the cellular response to BMP signaling in both mesoderm and NC at those two different stages. Enhanced mesodermal BMP signaling activates WNT signals, diffusing towards the ectoderm and essential for NB induction. The BMP signaling cascade remains functional in absence of Fhl3 since Fhl3 depletion was compensated by increasing response to BMPs by alternative other means (caBMPR, caSmad1): Fhl3 is an accessory enhancer of BMP signaling. Similar dispensable enhancing roles have been described for Fhl2 on WNT signaling (Labalette et al., 2004). In neurula-stage prospective NC or non-neural ectoderm, Fhl3 regulated both BMP and WNT signaling simultaneously, suggesting that Fhl3 mode of action may be broadly used in embryos. In addition, the incomplete rescue of NB/NC induction by increasing BMP signaling suggests that Fhl3 may also interfere with other pathways in the NB/NC-GRN. In contrast, both caBMPR and caSmad1 efficiently rescued *wnt8* gene expression suggesting a strong link between Fhl3 levels and *wnt8* transcriptional response to BMPs.

By direct measure of Fhl3 impact on the intracellular response to the extracellular gradient of BMP signaling in the mesoderm and in the prospective NB ectoderm in gastrulas (Figure 5), we found that Fhl3 was essential to ensure a high level response in the paraxial mesoderm, at similar levels to those observed in the ventral mesoderm, which is subjected to higher BMP signals. This high mesodermal response then controlled the high WNT signal activation essential for NB induction (LaBonne et al., 1998; Steventon et al., 2009). Simultaneously, the prospective NB ectoderm with low Fhl3, although adjacent to the paraxial mesoderm and subjected to the same intermediate levels of extracellular BMP,

348 responded at basal levels allowing early NB neuralization (Piacentino and Bronner, 2018).
349 Thus, Fhl3 tissue-specific expression elicits a differential response to the common external
350 intermediate BMP levels. Our results demonstrate how mesodermal Fhl3 activity controls the
351 low BMP/high WNT signaling levels inducing the NB state in the ectoderm during
352 gastrulation. During neurulation in contrast, elevated BMP and WNT signals cooperate with
353 NB transcription factors such as Pax3, Tfap2a and Zic1, to activate the premigratory NC
354 program (Monsoro-Burq et al., 2005; Sato et al., 2005; Simões-Costa et al., 2015; Steventon
355 et al., 2009; Wu et al., 2011). Fhl3 expression in premigratory NC cells promoted WNT
356 signaling in a Smad-dependent manner thus coordinating the high BMP/high WNT signaling
357 required for premigratory NC specification.
358
359 **Limitations of the study.**
360 ***Mechanisms of BMP signaling enhancement by Fhl3 and challenges in detecting Fhl3***
361 ***interactions with Smad proteins in vitro.***
362 Intense research has explored the BMP signaling cascade highlighting many actors
363 and modulators (Massague 2005; Piacentino and Bronner, 2018; Wu et al., 2011). We have
364 tried to narrow-down the mechanisms allowing Fhl3 to enhance BMP response. *In vivo* and
365 *in cellulo* assays support a model where Fhl3 binds to Smad1 or Smad4 and is present on
366 target genes BRE (*wnt8, ventx1.1*; Figures 4, S5). In HEK293 cells, two-hybrid assay shows
367 protein-protein interactions between Fhl3 and Smad1/4. In embryos, Fhl3 is bound to BREs
368 in a BMP-dependent manner by chromatin immunoprecipitation. Moreover, efficient binding
369 of Smad1 to its target sequences (*wnt8, ventx1.1)* depends on the levels of Fhl3. However,
370 we only detected a weak interaction between Fhl3 and Smad1 by direct immunoprecipitation.
371 This suggests that the two proteins could be part of a larger complex, which is found *in vivo*
372 and remains to be defined biochemically. Secondly, the subcellular localization of the Fhl3-
373 Smad first interaction remains unknown: our data suggest that Fhl3 may facilitate Smad
374 nuclear shuttling. Indeed, Fhl3 is enriched in the nucleus of AC cells with high BMP activity
375 (Figure 4). Moreover, transfection of Fhl3 in HEK293 cells promotes Smad1 nuclear

enrichment (Figure S5). However, an analysis of Smad nuclear shuttling dynamics by fluorescence recovery after photobleaching (FRAP), of Fhl3-Smad interactions by Proximity Ligation Assay, or of the enhancement of Fhl3-Smad interaction by BMP in the mammalian two-hybrid assay, all coupled to Fhl3 protein domains' mutagenesis, would allow the full demonstration of this model.

Conclusion

Altogether, our experiments suggest model where the scaffold LIM-domain protein Fhl3 would interact with Smad1/4 and promote the transcriptional activation of *wnt8* and other BMP targets such as *ventx1.1*, in a broad register of cell types including the NC, the paraxial mesoderm and the ectoderm lineages. The enhancement/facilitation of Smad activity by Fhl3 is reminiscent of the synergistic co-activator function of Fhl2 on CBP-p300 and β-catenin in cell lines (Labalette et al., 2004).

Fhl3 is a novel agonist of BMP signaling during development, cell-autonomously promoting Smad transcriptional activity during mesoderm and NC patterning. The developmental dynamics and tissue-specific expression of Fhl3 at different stages of the NC-GRN regulate the specific response of either mesoderm or ectoderm cells to the intermediate BMP levels controlling NC development, and coordinates BMP and WNT signaling. In the global view of early development, our findings highlight how complex patterns are refined locally in vertebrate embryos, following the initial and broad dorsal-ventral patterning. The cooperation between dorsal (Fhl3) and ventral (BMP) cues positions a secondary WNT-secreting signaling center in the paraxial mesoderm, sending the WNT signals towards an ectoderm area neuralized by low BMP signaling. The strictly controlled and coordinated signals ultimately induce the neural crest.

Acknowledgments.

We deeply thank Drs Liu, Theveneau, Sittewelle and Scerbo for comments, S. Dodier (histology), E. Belloir and C. Lantoine (animal husbandry), L. Besse and C. Messaoudi (image analysis) and XRCR (plasmids). Funding: Agence Nationale pour la Recherche

(ANR-15-CE13-0012-01-CRESTNETMETABO), Fondation pour la Recherche Médicale (DEQ20150331733), Institut Universitaire de France. Due to space limits, we apologize for not quoting more important references.

Authors contribution

M.A. PhD supervision: P.P., A.H.M-B; Analyses, Visualization: M.A., A.H.M-B; Investigation: M.A; Original Draft: M.A., P.P., A.H.M-B; Editing and Funding: A.H.M-B.

Declaration of interest

The authors declare no competing interests.

Figure Legends

Figure 1. Fhl3 is required for NB and NC induction *in vivo*

A: *Fhl3* expression is compared to neural plate/tube (np/nt), NB (nb) and NC (n) marker patterns during frog development. n, notochord; bl, blastocoel; m, paraxial mesoderm; e, endoderm.

B-F: *Fhl3* depletion prevents NB and NC but not neural (*sox2*) and mesoderm (*tbxt)* gene activation. It blocks NC migration and cranial cartilage formation.

G: *Fhl3* GOF reduces NP size (*sox2*), expands NB (*pax3*) and affects NC (*snai2)*. Due to NP reduction, NC is closer to the midline (dotted line) as seen after caBMPR1 injection. Blue/green lines measure width on the uninjected or injected (*) sides respectively.

Biological triplicates or more. The most frequent phenotype is shown; phenotype quantification in Table 1. Scale bars: 500 µm. See Figures S1-S2-S3A.

Figure 2. Fhl3 is necessary for BMP signaling and WNT-dependent NC induction by the mesoderm

A-B: Fhl3 is essential for BMP activity in late gastrula paraxial mesoderm.

C: In mesoderm (DLMZ)/ectoderm (AC) NC-inducing assay, depleting Fhl3 selectively in the mesoderm affects NB/NC induction in the ectoderm, a phenotype partially rescued by *ca-smad1* or *caBMPR* co-injection in the mesoderm.

D: In DLMZ/AC assay, WNT target expression (*axin2*) and TOPFLASH WNT reporter activity are decreased in wild-type AC juxtaposed to *fhl3* morphant DLMZ. FGF target expression (*dusp5*) is unchanged.

E: WNT reporter-injected ectoderm shows decreased response when juxtaposed to a *fhl3* morphant DLMZ, compared to a control DLMZ.

F: Injection of either *TCF3* or *wnt8* mRNAs in the ectoderm rescues NC induction in AC juxtaposed to *fhl3* morphant DLMZ.
Biological triplicates (or more, A-B, D-F) or duplicates (C). Data are represented as mean +/- S.E.M. See Figure S3A.

Figure 3. Fhl3 is necessary for NC specification in the ectoderm, downstream of NB formation

A-B: In a direct NC induction assay**,** key NC specifiers are poorly induced in *fhl3* morphant iNC compared to control.
C: BMP and WNT activities are reduced in *fhl3* morphant iNC.
D: Injection of *ca-smad1* or *wnt8* rescues NC induction in *fhl3* morphant iNC.
E: *Wnt8* and *axin2* expression are rescued by *ca-smad1* or *caBMPR* either in morphant iNC or in *fhl3* morphant recombinants.
Biological triplicates (or more, A-D) or duplicates (E). Data are represented as mean +/- S.E.M. See Figure S4.

Figure 4. Fhl3 interacts with Smad1/5/8 and enhances Smad-binding to *wnt8* promoter.
A: *Wnt8* expression decreases in *fhl3* morphant mesoderm *in vivo* after unilateral injection (*, decrease in 96% of cases, arrow) while *wnt8* is symmetrical in 93% of control siblings. Fhl3 and Smad1 bind to BS1 but not mutated BS1 (EMSA, shifted wt-BS1 primer pointed by arrow). At late gastrula stage *in vivo*, Fhl3 binds to BS1, BS2 and to v*entx1.1* BRE but not to EF1a sequences. In presence of Noggin, Fhl3 binding on those sequences is strongly reduced. Scale bar 500 µm.
B: Smad1 binding to BS1, BS2 and *ventx1.1-BRE* was analyzed either alone or after Fhl3 KD or GOF. Smad1-bound chromatin enrichment depended upon Fhl3 levels on all three promoter elements.
C: Fhl3 is found in the nucleus of BMP-positive animal cap cells. FHL3 nucleus/cytoplasm ratio is strongly decreased in Noggin-treated cells. See Figure S5A.
D: Modest Fhl3 enrichment by co-immunoprecipitation (Smad1-FLAG IP).
E: Strong direct protein-protein interactions between Fhl3 and Smad 1,2,4, by a mammalian two-hybrid reporter assay.
Biological triplicates or duplicates (Fhl3-FLAG/noggin CHIP, Smad1-FLAG/Fhl3 MO/mRNA ChIP and EMSA). Data are represented as mean +/- S.E.M. See Figure S5B.

Figure 5. Direct measurement of BMP signaling output in isolated ectoderm or mesoderm explants evidences specific Fhl3 requirement in the paraxial mesoderm for high BMP response.

A: Direct impact of Fhl3 levels was measured in AC. Increasing doses of Fhl3 mRNA promoted a dose-dependent BMP response while increasing Fhl3 MO gradually decreased the reporter response.
B: Fhl3 role in the BMP-responsive mesoderm was directly assessed by dissection and separate analysis of each type of tissue. High BMP response is seen in VMZ and DLMZ, while DMZ shows lower response (set to basal level). In contrast to the dorsal and ventral mesoderm, Fhl3 depletion specifically affects BMP activity in the dorsal-lateral mesoderm, changing the high response to background level response.
C: Prospective dorsal-lateral NB ectoderm (DL-EC) displays a basal-level response to BMPs (same scale as in B). Fhl3 KD affects BMP activity in the dorsal-lateral mesoderm (DLMZ) but not the adjacent DL-EC.
D: Model of Fhl3 role during of NB induction, resulting in low BMP/high WNT signaling in the prospective NB ectoderm. During gastrulation, combined activity of the ventral-dorsal BMP gradient and of dorsally-expressed Fhl3 positions the NC-inducing signaling center, secreting high levels of Wnt8 in the paraxial mesoderm located underneath the NB ectoderm.
Biological triplicate or more. Data are represented as mean +/- S.E.M.

STAR Methods Text

RESOURCE AVAILABILITY

Lead Contact

Further information and requests for resources and reagents should be directed to and will be fulfilled by the lead contact, Anne H. Monsoro-Burq; anne-helene.monsoro-burq@curie.fr.

Materials availability

Plasmids and materials generated in this study will be available upon request to the lead contact. Newly generated reagents are listed in Key Resources Table.

Data and code availability

This study did not generate any unique datasets or code.

EXPERIMENTAL MODEL DETAILS

Xenopus laevis embryos

Ovulation, *in vitro* fertilization and embryo culture were performed using standard methods (www.xenbase.org). Embryos were staged according to Nieuwkoop and Faber table (NF stage). All procedures were performed according to the European animal use and care law (animal care and housing approval license #C91-471-108, Direction Départementale de

Protection de la Population, Courcouronnes, France). Stages were described as follows: early gastrula = NF stage 10.5; late gastrula = stage 12; mid neurula = NF stage 14-15; NT closure late neurula = NF stage 18), tailbud =(NF stage 25), tadpole (NF stage > 30).

HEK293 cells

HEK293 cells were maintained under standard conditions, 5%CO_2, 37°C, in DMEM with 10% heat-inactivated fetal bovine serum, penicillin (100 U/ml) and streptomycin (100 μg/ml).

METHOD DETAILS

Sub-cloning of *Xenopus laevis fhl3* cDNA

An *fhl3* expression vector was obtained by amplifying the full-length *fhl3* cDNA by PCR from late neurula stage whole embryo cDNA and inserting it into pGEM-T Easy by TA cloning (Promega). The insert was then subcloned into pCS107 (*Not*I site). *Fhl3* PCR primers are listed in Key Resources Table.

***In vivo* gene depletion, gain of function (GOF) and rescue experiments**

For knockdown experiments, two antisense morpholino oligonucleotides (MO) were used to block *fhl3* translation or splicing (GeneTools). 15 ng of control MO or *fhl3* MO (either ATG MO or splice MO) were injected into one or two blastomere(s) of two-cell stage embryos, according to the assay. For Pax3 depletion experiments, 20 ng of previously validated MO (Monsoro-Burq et al., 2005) was injected into one blastomere of a two-cell stage embryo.

Capped mRNAs were synthesized using mMessage mMachine SP6 /T7 kits (Invitrogen). For Pax3 and Fhl3 GOF experiments, *pax3* mRNA (75 pg) or fhl3 mRNA (400-1000 pg) was injected into one blastomere at two/four-cell stage. For rescue experiments, h*FHL3* mRNA (300 pg) was co-injected with the *fhl3* MO into one blastomere of two-cell stage embryos; caSmad1 (3SD) mRNA (200 pg) or caBMPR1 mRNA (200 pg) or TCF3 mRNA (80 pg) or Wnt8 mRNA (100 pg) were co-injected with the *fhl3* MO into both blastomeres of two-cell stage embryos.

In each case, the injected blastomeres were traced by β-gal mRNA (250pg) or GFP mRNA (200pg) co-injection to mark the injected side (marked by an asterisk).

For CRIPSR/cas9 experiments, *fhl3* gRNA was synthesized using MEGAshortscript T7 transcription kit. Cas9 protein (2.5 ng) and *fhl3* sgRNA (300 pg) were co-injected into one blastomere of two-cell stage embryos.

Neural crest (NC) induction in mesoderm/ectoderm recombination assay

To recombine mesoderm at NC-inducing stage to a responsive "naive" ectoderm, a heterochronic recombination was used (Bonstein et al., 1998). Animal caps were dissected out from blastula stage embryos (stage 9), dorsal-lateral marginal zone (DLMZ) explants were dissected out from early gastrula stage embryos (stage 10.25). The two tissues were juxtaposed to form ectoderm-mesoderm recombinants and cultured in ¾ NAM (Slack and Forman, 1980) until sibling embryos reached the late neurula stage (stage 18).

Direct neural crest induction (iNC)

Animal cap ectoderm are pluripotent cells that respond to Pax3/Zic1 by activating a *bona fide* NC development (Milet et al., 2013). For this induced Neural Crest (iNC) assay, *pax3-GR* mRNA (35 pg) and *zic1-GR* mRNA (72 pg) synthesized with mMessage mMachine kits (Invitrogen), were co-injected into both blastomeres of two-cell stage embryos, with or without 15 ng *fhl3* MO. For rescue experiments, *caSmad1* (200 pg) or *wnt8* mRNA (100 pg) were co-injected with *pax3-GR* mRNA, *zic1-GR* mRNA and *fhl3* MO. Animal cap explants were dissected out at stage 9 and dexamethasone (or its solvent ethanol as a control) was added at stage 10.5. Explants were lysed at stage 18.

Whole mount *in situ* hybridization (WISH) and sectioning

Embryos were stained using a fast whole-mount *in situ* hybridization protocol (Monsoro-Burq, 2007). *Pax3*, *tfap2a*, *msx1* and *zic1* are expressed in the neural border and *snai2*, *foxd3*, *twist1* and *sox10* are expressed in the neural crest. *Sox2* is a general neural plate and neural tube marker and *epK* is a non-neural ectoderm marker. *Tbxt (xbra)* is a general mesoderm marker. *Myod* and *myf5* are expressed in the paraxial-fated mesoderm.

Late gastrula (stage 12.5), mid-neurula (stage 15) and late neurula (stage 18) embryos are shown in dorsal views with anterior to the top, except for the late gastrula stage embryo stained with *tbxt* shown in vegetal view, dorsal to the top (Figure 1A-C). The blastopore of late gastrulas is marked by a white dashed circlet. The dotted lines in Figure 1A, C, G indicate the midline. Tailbud stage embryos are seen in side views, anterior to the left. A sagittal view of a dissected late gastrula embryo is shown in the top right panel in Figure 1A. Mid- and late neurula embryos were embedded in paraffin and 12-µm-thick microtome transverse sections were cut (Figures 1, S1, S2).

Cartilage staining

Stage 45 tadpoles were fixed, dehydrated and stained in Alcian Blue for 24 hours. After several washes in ethanol until no blue stain is released, embryos were rehydrated, cleared with 4% KOH and transferred into graded glycerol solution in 2% KOH. Finally, ventral head cartilage was dissected. Whole tadpoles are shown from the dorsal side, anterior to the top

588 and the matching dissected cartilages are viewed from the ventral side, anterior to the top
589 (Figure 1F).
590
591 **Luciferase assay**
592 Each assay was repeated for biological replicates (each point on the graphs), each replicate
593 using the number of explants per condition indicated below.
594 For BMP reporter assay after Fhl3 depletion in Figures 2B, 5A-C, Renilla luciferase DNA
595 (pRL; Promega, 25 pg) and BMP reporter DNA (pGL2-15xGCCCG-lux; 50 pg) were co-
596 injected into both blastomeres at two-cell stage with or without *fhl3* MO (7.5 ng/10nl or 15
597 ng/10nl). Twenty animal caps were dissected at stage 9 per sample; or 20 mesoderm
598 explants either DMZ, or DLMZ, or VMZ or DL-EC were dissected at stage 10.5 per sample.
599 All explants were grown individually in ¾ NAM, pooled (at stage 18 for animal caps and at
600 stage 12.5 for mesoderm explants) and lysed in 60 µl of Passive lysis buffer (Promega). For
601 the BMP reporter dose-response experiment after Fhl3 GOF (Figure 5A), each blastomere at
602 two-cell stage was co-injected with Renilla luciferase DNA (25pg), BMP reporter DNA (50pg)
603 and *noggin* mRNA (0.2pg) with or without *fhl3* mRNA (400 pg or 1ng per cell), and 20 animal
604 caps per sample were prepared as described above.
605 For WNT reporter assay in ectoderm/mesoderm recombinants (Figure 2E), Renilla luciferase
606 DNA (25 pg) and WNT reporter DNA (TOPFLASH, 50 pg) were co-injected into both
607 blastomeres at two-cell stage. Animal cap (ectoderm) explants were dissected at stage 9 and
608 juxtaposed to control or Fhl3-depleted DLMZ. Fifteen (15) recombinants
609 (ectoderm+mesoderm) were grown individually then lysed in 60 µl Passive lysis buffer at
610 stage 18.
611 For BMP and WNT reporter assays in iNC (Figure 3C), Renilla luciferase DNA (25 pg), *pax3-*
612 *GR* mRNA (35 pg) and *zic1-GR* mRNA (72 pg) were co-injected with either BMP reporter
613 DNA (50 pg) or WNT reporter DNA (50 pg) into both blastomeres at two-cell stage with or
614 without 15 ng of *fhl3* MO. Twenty animal cap (ectoderm) explants were dissected out from
615 stage 9 embryos and lysed in 60 µl of Passive lysis buffer at stage 18.
616 In all assays, Firefly and Renilla luciferase activities were measured using the Dual-Glo
617 Luciferase Assay System (Promega).
618
619 **qRT-PCR**
620 Total RNA was extracted using Phenol/Chloroform/Isoamyl Alcohol from *Xenopus laevis*
621 embryos or tissue explants at late neurula stage (stage 18). We used M-MLV reverse
622 transcriptase for reverse transcription and SYBR Green mix (BIO-RAD) for quantitative RT-
623 PCR. Results were normalized against the reference genes *odc* and *ef1a*. For primers
624 sequences see Key Resources Table.

Chromatin immunoprecipitation (ChIP)

Embryos were injected in both blastomeres at two-cell stage with mRNA encoding FLAG-Smad1 (200 pg) and FLAG-Fhl3 cDNA separately (200 pg) or FLAG-Fhl3 cDNA with noggin mRNA (25 pg). Injected embryos were collected at late gastrula stage (stage 12, 80-100 embryos per sample) and processed according to Wills et al., 2014. Sonication was performed using a 3.2 mm tapered microtip for 13 mm horn (Branson 450 sonicator). Anti-FLAG antibodies coupled to magnetic beads (42 µg) were added to the chromatin. Quantitative PCR was performed on the immunoprecipitated and fragmented chromatin using primers amplifying *wnt8, ef1a* (background control) or *ventx1.1* promoter regions (positive control). W*nt8* promoter primers amplified the two following elements where putative Smad binding sites are underlined:

BS1:AGCTCACCAAGTTGATCATGTGGTCCAGGTGCACCAGTCC***TAGAC***CCCTAACCAC GGGTCGTGGAAAACTGAA;

BS2:CCTTCCAGTAGAAAAACTCATGTCAATACACATATATAGGCTACAAGAGATAACCAT CGG***CAGAC***AAGGCTCACCTTGGTTTCACCA. Data were analyzed by the ΔΔC(t) method. Once a threshold cycle (C(t)) number is calculated for each sample, ΔC(t) is calculated by normalizing the IP values to the input values for each condition by subtracting input values from each corresponding ChIP value [ΔC(t) = ChIP C(t) – Input C(t)]. ΔΔC(t) was next calculated by subtracting the ΔC(t) for uninjected samples from the ΔC(t) for experimental samples [$\Delta\Delta C(t) = \Delta C(t)_{experimental} - \Delta C(t)_{uninjected}$]. Once ΔΔC(t) was determined, the fold change between samples was determined by using the formula [Fold Change (FC) = $2^{[-\Delta\Delta C(t)]}$] (Taneyhill and Adams, 2008). Primers and FLAG antibody are listed in Key Resources Table.

Electrophoresis mobility shift assay (EMSA)

HEK293 cells, which do not express endogenous Fhl3, were used to test nuclear protein binding to the BS1 oligonucleotide. To this end, cells were transfected with plasmids encoding *gfp, smad1* or *fhl3*. Nuclear extracts contained an EDTA-free protease inhibitor cocktail to avoid Zn^{2+} chelation, Zn^{2+} being necessary for the maintenance of FHL3 structure. Oligonucleotides containing a wild-type or a mutated form of a BMP-responsive element (see sequence in Key Resources Table) were labeled with biotin (Biotin 3' End DNA labeling kit, Thermo Scientific), annealed and incubated with nuclear protein extracts from HEK293T cells in 50 ng/µL Poly [dI·dC], 2.5% glycerol, 5 mM MgCl2 and 0.05% NP-40 diluted in EMSA binding buffer (LightShift Chemiluminescent EMSA Kit, Thermo Scientific) during 20 min at RT. Complexes were separated on a 5% polyacrylamide gel and transferred to a nylon

membrane (Hybond-N+, Amersham). Biotin-labeled DNA was detected by chemoluminescence according to manufacturer's instructions.

Mammalian two-hybrid assay

For a two-hybrid system adapted to eukaryotes, we used the Check-Mate Mammalian Two-Hybrid System (Promega). Using Gibson cloning method, human Fhl3 was sub-cloned into the pBind vector, which contains the yeast GAL4 DNA-binding domain and human Smad1, 2 and 4 were cloned into the pACT vector, which contains the herpes simplex virus VP16 activation domain and a nuclear localization sequence. A luciferase reporter driven by five GAL4 binding-sites (pG5-luc) was co-transfected into HEK293T cells. Luciferase activity was measured using the Dual-Glo Luciferase Assay system (Promega). Fhl3-Smad2 interactions serve as a positive control (Ding et al., 2009).

Western blot

Detection of phospho-Smads. 10 to 15 DLMZ explants were dissected at stage 10.5, cultured individually and lysed when sibling embryos reached stage 12.5 in presence of phosphatase inhibitor (PhosphoSTOP, Roche) and protease inhibitors (Sigma) and analyzed by western blotting. ECL signal was quantified using ImageJ. Antibodies are listed in Key Resources Table.

Assessment of phospho-SMAD dynamics. HEK-293 cells, known to respond to BMP4, were transfected either with GFP or with human FHL3. After 5 hours of starving in serum-free medium, they were incubated with 10 ng/ml BMP4 during 15 min to longer. Proteins extracted at various times were analyzed by western blotting.

Detection of nuclear FHL3 (Figure S5A). HEK-293 were transfected with plasmids encoding GFP, SMAD1, caSMAD1 or FHL3.Two days after transfection, cells were starved for 6 hours. One condition with FHL3 transfection was then incubated with 10 ng/ml BMP4 during 30 min. Nuclear proteins were extracted for western blotting with a standard protocol. Western blot signals were measured using the relative signal intensity of nuclear Fhl3 or phospho-Smad1/58 compared to Histone H3 baseline and quantified using ImageJ.

Immunoprecipitation

Total proteins were extracted using RIPA buffer (100mM NaCl, 0,5% NP40, 20mM Tris-HCl pH 7,5, 5mM $MgCl_2$, protease inhibitors and phosphatases inhibitors) from HEK293 cells transfected with plasmids encoding Smad1-FLAG, Fhl3-HA or both (4 µg) or from *X. laevis* embryos injected with Smad1-FLAG mRNA (200 pg), Fhl3-HA plasmids (50 pg) or both. All samples were immunoprecipitated with either 40 µl of FLAG-M2 magnetic beads (Sigma M8823) or 5 µg HA antibody mixed with 40 µl Dynabeads Protein A (Invitrogen) previously

washed in RIPA. All samples were incubated with agitation overnight at 4°C. Beads were then washed five times in RIPA buffer. Inputs and immunoprecipitated fractions were analyzed by immunoblotting (see Key Resources Table for antibodies and reagents).

Imaging and image processing

WISH images were taken using a Lumar V12 Binocular microscope equipped with bright field or fluorescent filters and color camera (Zeiss), and were processed using Photoshop or Affinity Photo. Live imaging was done on animal caps or HEK293 cells using Leica SP8 confocal microscope with a 63x immersion objective. Confocal stacks were analyzed using ImageJ software.

For image fluorescence quantification, the cells expressing Fhl3-GFP were stained by the nuclear marker DAPI and the actin filaments marker Phalloidin. Using an ImageJ macro developed by the Curie CoreTech microscopy platform, we delineated cell and nucleus boundaries (using phalloidin staining / cytoplasmic GFP fluorescence and DAPI staining respectively). This allowed measuring fluorescence intensities and automatically calculated nucleus/cytoplasm GFP ratios. All ImageJ plugings are available upon request. In Figure 4C: The normalized fluorescence intensity ratio between nucleus and cytoplasm was measured in 20 injected ectoderm cells for each condition.

QUANTIFICATION AND STATISTICAL ANALYSIS

All experiments were performed at least in biological triplicates, except the rescue experiment in Figure 2C and the *axin2* and *wnt8* rescue in the recombinant experiment in Figure 3E, and the ChIP experiments (Fhl3-FLAG + noggin) and (Smad1-FLAG + Fhl3 MO/mRNA) (Figure 4A-B), which were performed in biological duplicates. Each dot on the graphs represents one independent experiment (biological replicate). Each sample for reporter assays comprises 10-15 individual explants dissected from sibling embryos. Each sample for ChIP comprises 60-80 sibling embryos. For in situ hybridization, examples of embryos with the most frequent phenotypes are shown, full quantification of the phenotypes is provided in Supplementary materials. We used Prism for statistical analysis, error bars represent S.E.M., Student's *t*-test was used to determine statistical significance between two groups and One-way ANOVA test was used for comparison among three groups or more (Figures 2E, 2F, 3B, 3D, 4E and 5A). (*$p<0.05$; **$p<0.01$; ***$p<0.001$, ns: not significant).

Figure 2 and 3: Each point on the graphs represents an independent biological replicate, each with 10-15 tissue explants dissected from sibling embryos and pooled together.

Figure 4 A,B: Each point on the graphs represents an independent biological replicate, each with ~80 sibling embryos per sample pooled together. C: each point represents one cell.

734 Figure 5: A-C: Each point on the graphs represents an independent biological replicate, each
735 with 10-12 tissue explants dissected from sibling embryos and pooled together.

References

Aoki, Y., Saint-Germain, N., Gyda, M., Magner-Fink, E., Lee, Y.-H., Credidio, C., Saint-Jeannet, J.-P., 2003. Sox10 regulates the development of neural crest-derived melanocytes in Xenopus. Dev. Biol. 259, 19–33. https://doi.org/10.1016/S0012-1606(03)00161-1

Bach, I., 2000. The LIM domain: regulation by association. Mech. Dev. 91, 5–17.

Bae, C.-J., Park, B.-Y., Lee, Y.-H., Tobias, J.W., Hong, C.-S., Saint-Jeannet, J.-P., 2014. Identification of Pax3 and Zic1 targets in the developing neural crest. Dev. Biol. 386, 473–483. https://doi.org/10.1016/j.ydbio.2013.12.011

Bier, E., De Robertis, E.M., 2015. BMP gradients: A paradigm for morphogen-mediated developmental patterning. Science 348, aaa5838. https://doi.org/10.1126/science.aaa5838

Blythe, S.A., Reid, C.D., Kessler, D.S., Klein, P.S., 2009. Chromatin Immunoprecipitation in Early Xenopus Laevis Embryos. Dev. Dyn. Off. Publ. Am. Assoc. Anat. 238, 1422–1432. https://doi.org/10.1002/dvdy.21931

Bonstein, L., Elias, S., Frank, D., 1998. Paraxial-fated mesoderm is required for neural crest induction in Xenopus embryos. Dev. Biol. 193, 156–168. https://doi.org/10.1006/dbio.1997.8795

Bradley, R.S., Espeseth, A., Kintner, C., 1998. NF-protocadherin, a novel member of the cadherin superfamily, is required for Xenopus ectodermal differentiation. Curr. Biol. CB 8, 325–334.

Chang, C., Hemmati Brivanlou, A., 1998. Neural crest induction by Xwnt7B in Xenopus. Dev. Biol. 194, 129–134. https://doi.org/10.1006/dbio.1997.8820

Christian, J.L., Gavin, B.J., McMahon, A.P., Moon, R.T., 1991. Isolation of cDNAs partially encoding four Xenopus Wnt-1/int-1-related proteins and characterization of their transient expression during embryonic development. Dev. Biol. 143, 230–234.

Cottle, D.L., McGrath, M.J., Cowling, B.S., Coghill, I.D., Brown, S., Mitchell, C.A., 2007. FHL3 binds MyoD and negatively regulates myotube formation. J. Cell Sci. 120, 1423–1435. https://doi.org/10.1242/jcs.004739

De Crozé, N., Maczkowiak, F., Monsoro-Burq, A.H., 2011. Reiterative AP2a activity controls sequential steps in the neural crest gene regulatory network. Proc. Natl. Acad. Sci. U. S. A. 108, 155–160. https://doi.org/10.1073/pnas.1010740107

De Robertis, E.M., Kuroda, H., 2004. Dorsal-ventral patterning and neural induction in Xenopus embryos. Annu. Rev. Cell Dev. Biol. 20, 285–308. https://doi.org/10.1146/annurev.cellbio.20.011403.154124

772 Ding, L., Wang, Z., Yan, J., Yang, X., Liu, A., Qiu, W., Zhu, J., Han, J., Zhang, H., Lin, J.,
773 Cheng, L., Qin, X., Niu, C., Yuan, B., Wang, X., Zhu, C., Zhou, Y., Li, J., Song, H.,
774 Huang, C., Ye, Q., 2009. Human four-and-a-half LIM family members suppress tumor
775 cell growth through a TGF-β–like signaling pathway. J. Clin. Invest. 119, 349–361.
776 https://doi.org/10.1172/JCI35930
777 Douarin, N.L., Kalcheim, C., 1999. The Neural Crest. Cambridge University Press.
778 Elkouby, Y.M., Elias, S., Casey, E.S., Blythe, S.A., Tsabar, N., Klein, P.S., Root, H., Liu, K.J.,
779 Frank, D., 2010. Mesodermal Wnt signaling organizes the neural plate via Meis3.
780 Dev. Camb. Engl. 137, 1531–1541. https://doi.org/10.1242/dev.044750
781 Fuentealba, L.C., Eivers, E., Ikeda, A., Hurtado, C., Kuroda, H., Pera, E.M., De Robertis,
782 E.M., 2007. Integrating Patterning Signals: Wnt/GSK3 Regulates the Duration of the
783 BMP/Smad1 Signal. Cell 131, 980–993. https://doi.org/10.1016/j.cell.2007.09.027
784 Garnett, A.T., Square, T.A., Medeiros, D.M., 2012. BMP, Wnt and FGF signals are integrated
785 through evolutionarily conserved enhancers to achieve robust expression of Pax3
786 and Zic genes at the zebrafish neural plate border. Development 139, 4220–4231.
787 https://doi.org/10.1242/dev.081497
788 Garriock, R.J., Warkman, A.S., Meadows, S.M., D'Agostino, S., Krieg, P.A., 2007. Census of
789 vertebrate Wnt genes: isolation and developmental expression of Xenopus Wnt2,
790 Wnt3, Wnt9a, Wnt9b, Wnt10a, and Wnt16. Dev. Dyn. Off. Publ. Am. Assoc. Anat.
791 236, 1249–1258. https://doi.org/10.1002/dvdy.21156
792 Grammer, T.C., Liu, K.J., Mariani, F.V., Harland, R.M., 2000. Use of Large-Scale Expression
793 Cloning Screens in the Xenopus laevis Tadpole to Identify Gene Function. Dev. Biol.
794 228, 197–210. https://doi.org/10.1006/dbio.2000.9945
795 Han, W., Hu, P., Wu, F., Wang, S., Hu, Y., Li, S., Jiang, T., Qiang, B., Peng, X., 2018. FHL3
796 links cell growth and self-renewal by modulating SOX4 in glioma. Cell Death Differ.
797 https://doi.org/10.1038/s41418-018-0152-1
798 Harland, R., Gerhart, J., 1997. Formation and function of Spemann's organizer. Annu. Rev.
799 Cell Dev. Biol. 13, 611–667. https://doi.org/10.1146/annurev.cellbio.13.1.611
800 Hong, C.-S., Saint-Jeannet, J.-P., 2007. The Activity of Pax3 and Zic1 Regulates Three
801 Distinct Cell Fates at the Neural Plate Border. Mol. Biol. Cell 18, 2192–2202.
802 https://doi.org/10.1091/mbc.E06-11-1047
803 Hoppler, S., Moon, R.T., 1998. BMP-2/-4 and Wnt-8 cooperatively pattern the Xenopus
804 mesoderm. Mech. Dev. 71, 119–129. https://doi.org/10.1016/S0925-4773(98)00004-5
805 Hopwood, N.D., Pluck, A., Gurdon, J.B., 1989a. MyoD expression in the forming somites is
806 an early response to mesoderm induction in Xenopus embryos. EMBO J. 8, 3409–
807 3417.

808 Hopwood, N.D., Pluck, A., Gurdon, J.B., 1989b. A Xenopus mRNA related to Drosophila
809 twist is expressed in response to induction in the mesoderm and the neural crest. Cell
810 59, 893–903. https://doi.org/10.1016/0092-8674(89)90612-0
811 Kadrmas, J.L., Beckerle, M.C., 2004. The LIM domain: from the cytoskeleton to the nucleus.
812 Nat. Rev. Mol. Cell Biol. 5, 920–931. https://doi.org/10.1038/nrm1499
813 Kumar, S., Umair, Z., Yoon, J., Lee, U., Kim, S.C., Park, J.-B., Lee, J.-Y., Kim, J., 2018. Xbra
814 and Smad-1 cooperate to activate the transcription of neural repressor ventx1.1 in
815 Xenopus embryos. Sci. Rep. 8. https://doi.org/10.1038/s41598-018-29740-9
816 Kuriyama, S., Lupo, G., Ohta, K., Ohnuma, S.-I., Harris, W.A., Tanaka, H., 2006. Tsukushi
817 controls ectodermal patterning and neural crest specification in Xenopus by direct
818 regulation of BMP4 and X-delta-1 activity. Dev. Camb. Engl. 133, 75–88.
819 https://doi.org/10.1242/dev.02178
820 Kusanagi, K., Inoue, H., Ishidou, Y., Mishima, H.K., Kawabata, M., Miyazono, K., 2000.
821 Characterization of a Bone Morphogenetic Protein-responsive Smad-binding
822 Element. Mol. Biol. Cell 11, 555–565.
823 Labalette, C., Renard, C.-A., Neuveut, C., Buendia, M.-A., Wei, Y., 2004. Interaction and
824 functional cooperation between the LIM protein FHL2, CBP/p300, and beta-catenin.
825 Mol. Cell. Biol. 24, 10689–10702. https://doi.org/10.1128/MCB.24.24.10689-
826 10702.2004
827 LaBonne, C., Bronner-Fraser, M., 1998. Neural crest induction in Xenopus: Evidence for a
828 two-signal model. Development 125, 2403–2414.
829 Lamb, T.M., Harland, R.M., 1995. Fibroblast growth factor is a direct neural inducer, which
830 combined with noggin generates anterior-posterior neural pattern. Dev. Camb. Engl.
831 121, 3627–3636.
832 Li, B., Kuriyama, S., Moreno, M., Mayor, R., 2009. The posteriorizing gene Gbx2 is a direct
833 target of Wnt signalling and the earliest factor in neural crest induction. Dev. Camb.
834 Engl. 136, 3267–3278. https://doi.org/10.1242/dev.036954
835 Litsiou, A., Hanson, S., Streit, A., 2005. A balance of FGF, BMP and WNT signalling
836 positions the future placode territory in the head. Dev. Camb. Engl. 132, 4051–4062.
837 https://doi.org/10.1242/dev.01964
838 Massagué, J., Seoane, J., Wotton, D., 2005. Smad transcription factors. Genes Dev. 19,
839 2783–2810. https://doi.org/10.1101/gad.1350705
840 Meeson, A.P., Shi, X., Alexander, M.S., Williams, R.S., Allen, R.E., Jiang, N., Adham, I.M.,
841 Goetsch, S.C., Hammer, R.E., Garry, D.J., 2007. Sox15 and Fhl3 transcriptionally
842 coactivate Foxk1 and regulate myogenic progenitor cells. EMBO J. 26, 1902–1912.
843 https://doi.org/10.1038/sj.emboj.7601635

844 Milet, C., Maczkowiak, F., Roche, D.D., Monsoro-Burq, A.H., 2013. Pax3 and Zic1 drive
845 induction and differentiation of multipotent, migratory, and functional neural crest in
846 Xenopus embryos. Proc. Natl. Acad. Sci. U. S. A. 110, 5528–5533.
847 https://doi.org/10.1073/pnas.1219124110
848 Mizuseki, K., Kishi, M., Matsui, M., Nakanishi, S., Sasai, Y., 1998. Xenopus Zic-related-1 and
849 Sox-2, two factors induced by chordin, have distinct activities in the initiation of neural
850 induction. Dev. Camb. Engl. 125, 579–587.
851 Molenaar, M., van de Wetering, M., Oosterwegel, M., Peterson-Maduro, J., Godsave, S.,
852 Korinek, V., Roose, J., Destrée, O., Clevers, H., 1996. XTcf-3 transcription factor
853 mediates beta-catenin-induced axis formation in Xenopus embryos. Cell 86, 391–
854 399. https://doi.org/10.1016/s0092-8674(00)80112-9
855 Monsoro-Burq, A.H., 2007. A rapid protocol for whole-mount in situ hybridization on Xenopus
856 embryos. CSH Protoc. 2007, pdb.prot4809. https://doi.org/10.1101/pdb.prot4809
857 Monsoro-Burq, A.-H., Fletcher, R.B., Harland, R.M., 2003. Neural crest induction by paraxial
858 mesoderm in Xenopus embryos requires FGF signals. Dev. Camb. Engl. 130, 3111–
859 3124.
860 Monsoro-Burq, A.-H., Wang, E., Harland, R., 2005. Msx1 and Pax3 cooperate to mediate
861 FGF8 and WNT signals during Xenopus neural crest induction. Dev. Cell 8, 167–178.
862 https://doi.org/10.1016/j.devcel.2004.12.017
863 Nichane, M., de Crozé, N., Ren, X., Souopgui, J., Monsoro-Burq, A.H., Bellefroid, E.J., 2008.
864 Hairy2-Id3 interactions play an essential role in Xenopus neural crest progenitor
865 specification. Dev. Biol. 322, 355–367. https://doi.org/10.1016/j.ydbio.2008.08.003
866 Nieuwkoop P.D. and Faber Garland J., J.B., 1995. Normal table of Xenopus laevis (Daudin):
867 edited by P.D. Nieuwkoop and J. Faber Garland Publishing, 1994. Trends Genet. 11,
868 418. https://doi.org/10.1016/S0168-9525(00)89129-5
869 Pegoraro, C., Figueiredo, A.L., Maczkowiak, F., Pouponnot, C., Eychène, A., Monsoro-Burq,
870 A.H., 2015. PFKFB4 controls embryonic patterning via Akt signalling independently of
871 glycolysis. Nat. Commun. 6, 5953.
872 Piacentino, M.L., Bronner, M.E., 2018. Intracellular attenuation of BMP signaling via CKIP-
873 1/Smurf1 is essential during neural crest induction. PLOS Biol. 16, e2004425.
874 https://doi.org/10.1371/journal.pbio.2004425
875 Pla, P., Monsoro-Burq, A.H., 2018. The neural border: Induction, specification and
876 maturation of the territory that generates neural crest cells. Dev. Biol.
877 https://doi.org/10.1016/j.ydbio.2018.05.018
878 Plouhinec, J.-L., Medina-Ruiz, S., Borday, C., Bernard, E., Vert, J.-P., Eisen, M.B., Harland,
879 R.M., Monsoro-Burq, A.H., 2017. A molecular atlas of the developing ectoderm

880 defines neural, neural crest, placode, and nonneural progenitor identity in vertebrates.
881 PLoS Biol. 15, e2004045. https://doi.org/10.1371/journal.pbio.2004045
882 Plouhinec, J.-L., Roche, D.D., Pegoraro, C., Figueiredo, A.-L., Maczkowiak, F., Brunet, L.J.,
883 Milet, C., Vert, J.-P., Pollet, N., Harland, R.M., Monsoro-Burq, A.H., 2014. Pax3 and
884 Zic1 trigger the early neural crest gene regulatory network by the direct activation of
885 multiple key neural crest specifiers. Dev. Biol. 386, 461–472.
886 https://doi.org/10.1016/j.ydbio.2013.12.010
887 Plouhinec, J.-L., Zakin, L., Moriyama, Y., De Robertis, E.M., 2013. Chordin forms a self-
888 organizing morphogen gradient in the extracellular space between ectoderm and
889 mesoderm in the Xenopus embryo. Proc. Natl. Acad. Sci. U. S. A. 110, 20372–20379.
890 https://doi.org/10.1073/pnas.1319745110
891 Saint-Jeannet, J.P., He, X., Varmus, H.E., Dawid, I.B., 1997. Regulation of dorsal fate in the
892 neuraxis by Wnt-1 and Wnt-3a. Proc. Natl. Acad. Sci. U. S. A. 94, 13713–13718.
893 Sasai, N., Mizuseki, K., Sasai, Y., 2001. Requirement of FoxD3-class signaling for neural
894 crest determination in Xenopus. Dev. Camb. Engl. 128, 2525–2536.
895 Sato, T., Sasai, N., Sasai, Y., 2005. Neural crest determination by co-activation of Pax3 and
896 Zic1 genes in Xenopus ectoderm. Development 132, 2355–2363.
897 https://doi.org/10.1242/dev.01823
898 Schille, C., Bayerlová, M., Bleckmann, A., Schambony, A., 2016. Ror2 signaling is required
899 for local upregulation of GDF6 and activation of BMP signaling at the neural plate
900 border. Development 143, 3182–3194. https://doi.org/10.1242/dev.135426
901 Sieber, C., Kopf, J., Hiepen, C., Knaus, P., 2009. Recent advances in BMP receptor
902 signaling. Cytokine Growth Factor Rev. 20, 343–355.
903 https://doi.org/10.1016/j.cytogfr.2009.10.007
904 Simões-Costa, M., Stone, M., Bronner, M.E., 2015. Axud1 integrates Wnt signaling and
905 transcriptional inputs to drive neural crest formation. Dev. Cell 34, 544–554.
906 https://doi.org/10.1016/j.devcel.2015.06.024
907 Sive, 2000. Early Development of Xenopus laevis: A Laboratory Manual [WWW Document].
908 URL
909 https://www.cshlpress.com/default.tpl?cart=15415143921173291 23&fromlink=T&linka
910 ction=full&linksortby=oop_title&--eqSKUdatarq=855 (accessed 11.6.18).
911 Slack, J.M., Forman, D., 1980. An interaction between dorsal and ventral regions of the
912 marginal zone in early amphibian embryos. J. Embryol. Exp. Morphol. 56, 283–299.
913 Smith, J.C., Price, B.M., Green, J.B., Weigel, D., Herrmann, B.G., 1991. Expression of a
914 Xenopus homolog of Brachyury (T) is an immediate-early response to mesoderm
915 induction. Cell 67, 79–87. https://doi.org/10.1016/0092-8674(91)90573-h

916 Steventon, B., Araya, C., Linker, C., Kuriyama, S., Mayor, R., 2009. Differential requirements
917 of BMP and Wnt signalling during gastrulation and neurulation define two steps in
918 neural crest induction. Dev. Camb. Engl. 136, 771–779.
919 https://doi.org/10.1242/dev.029017
920 Suzuki, A., Ueno, N., Hemmati-Brivanlou, A., 1997. Xenopus msx1 mediates epidermal
921 induction and neural inhibition by BMP4. Dev. Camb. Engl. 124, 3037–3044.
922 Taneyhill, L.A., Adams, M.S., 2008. Investigating regulatory factors and their DNA binding
923 affinities through real time quantitative PCR (RT-QPCR) and chromatin
924 immunoprecipitation (ChIP) assays. Methods Cell Biol. 87, 367–389.
925 https://doi.org/10.1016/S0091-679X(08)00219-7
926 Wills, A.E., Gupta, R., Chuong, E., Baker, J.C., 2014. Chromatin immunoprecipitation and
927 deep sequencing in Xenopus tropicalis and Xenopus laevis. Methods San Diego Calif
928 66, 410–421. https://doi.org/10.1016/j.ymeth.2013.09.010
929 Wu, M.Y., Ramel, M.-C., Howell, M., Hill, C.S., 2011. SNW1 Is a Critical Regulator of Spatial
930 BMP Activity, Neural Plate Border Formation, and Neural Crest Specification in
931 Vertebrate Embryos. PLoS Biol. 9. https://doi.org/10.1371/journal.pbio.1000593
932

Alkobtawi et al., Figure 1

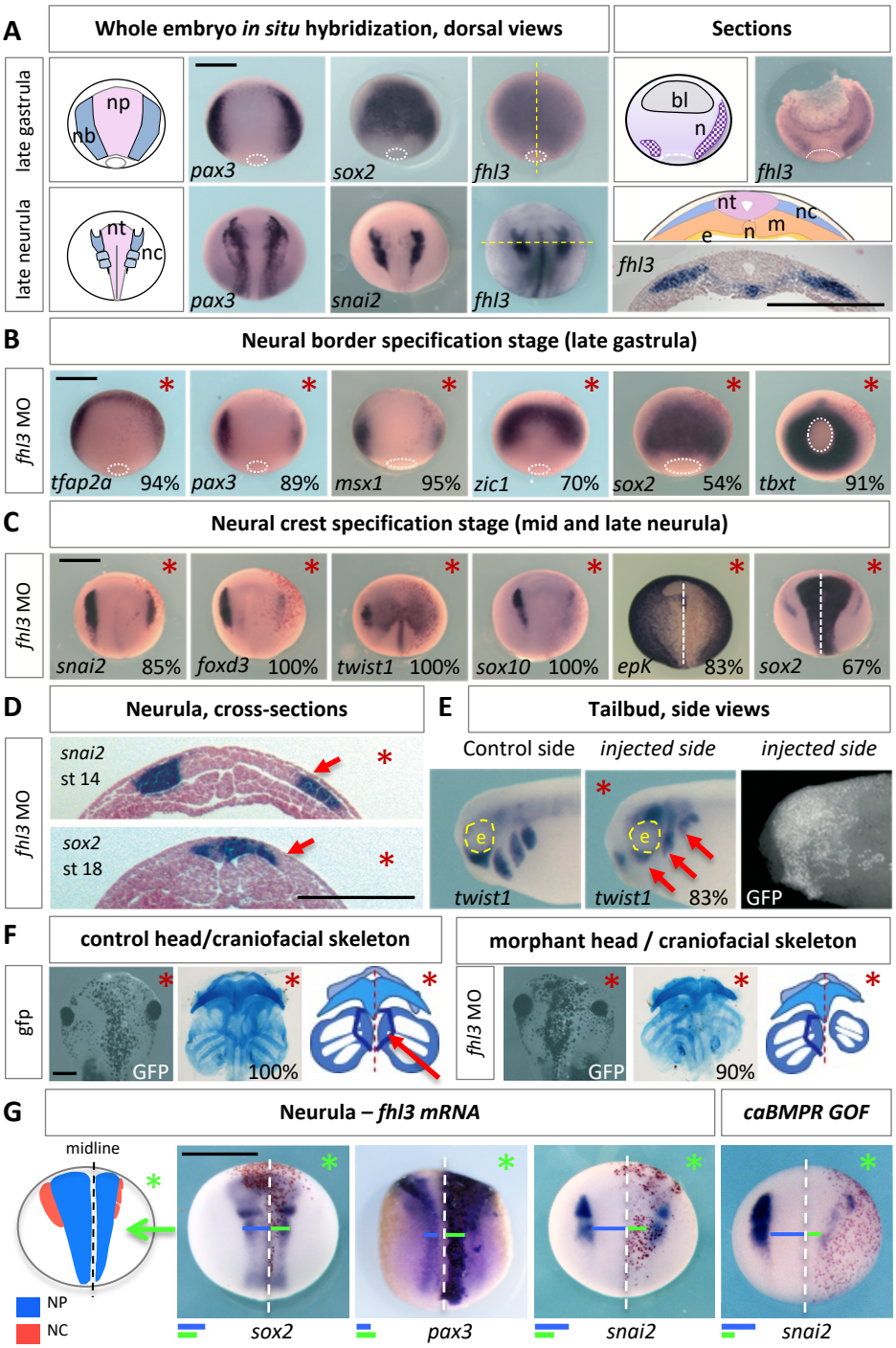

Alkobtawi et al., Figure 2.

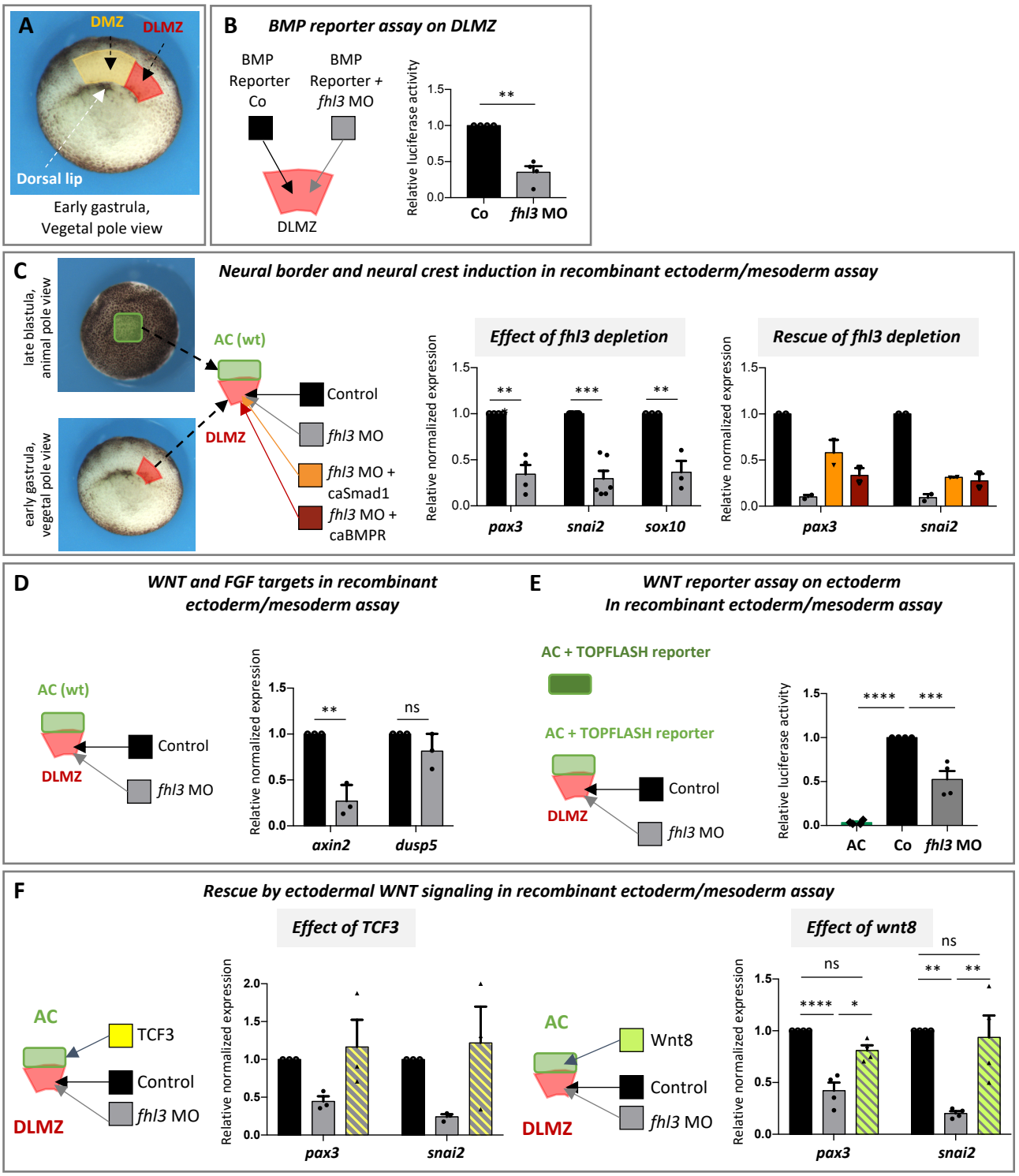

Alkobtawi et al., Figure 3

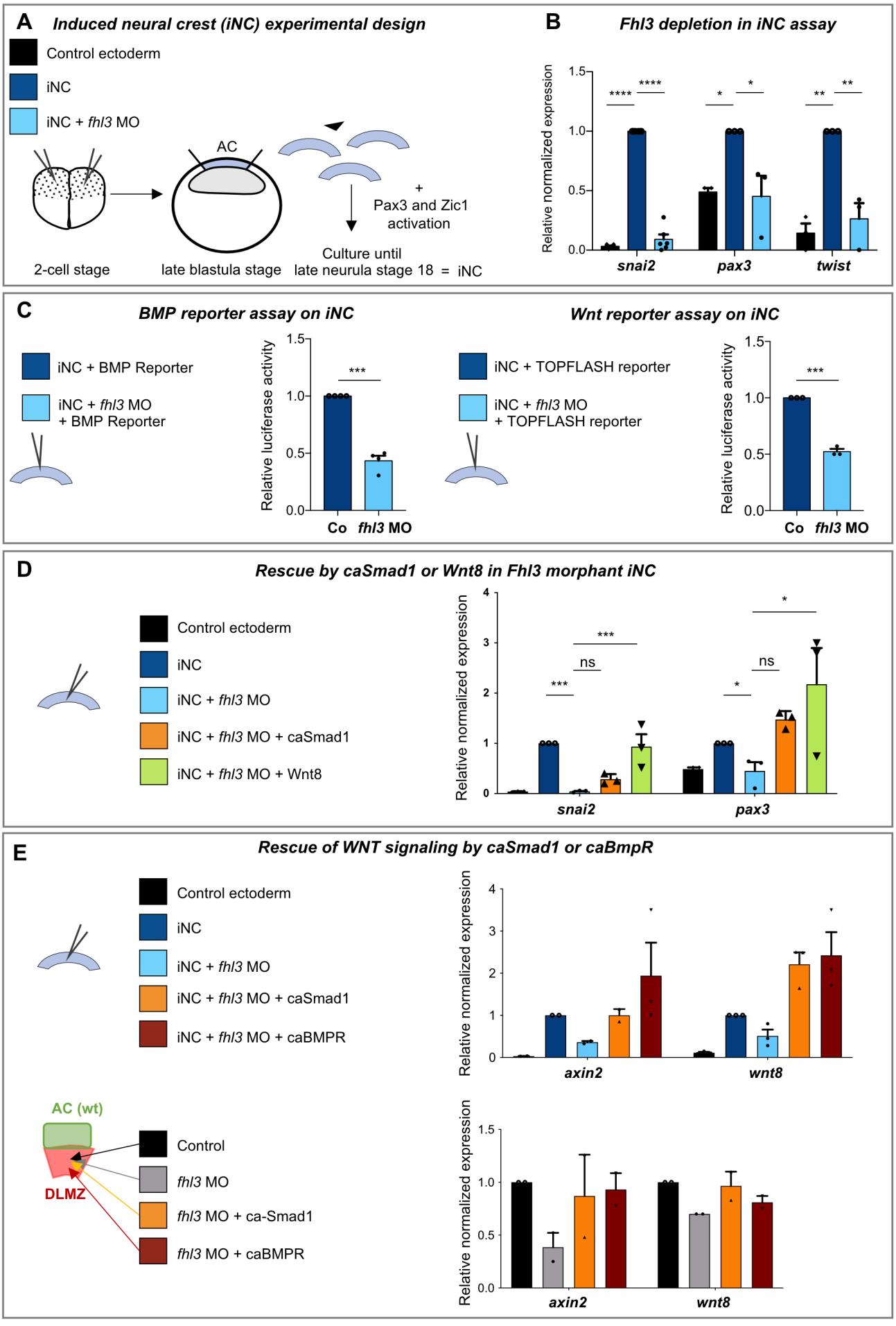

Alkobtawi et al. Figure 4.

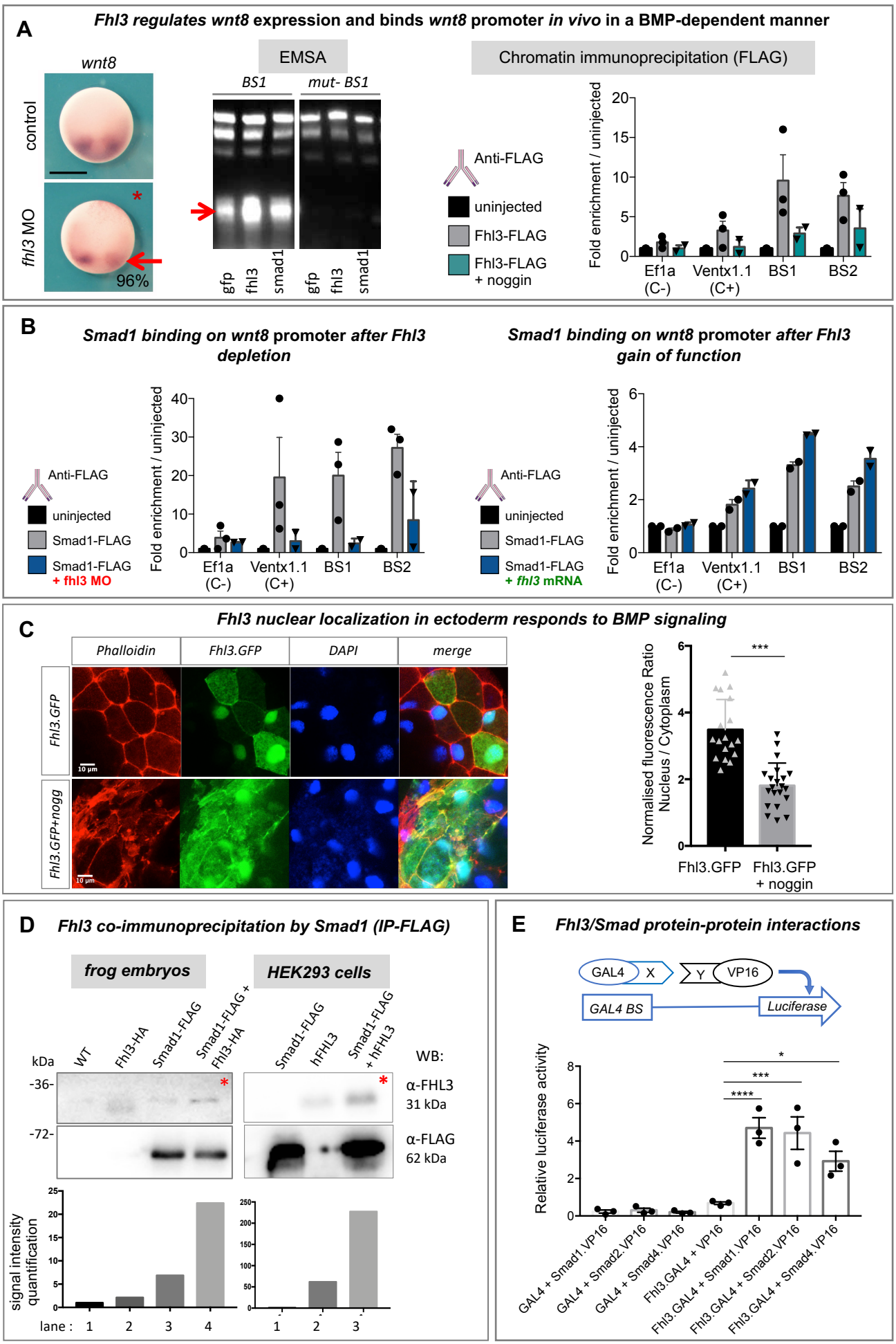

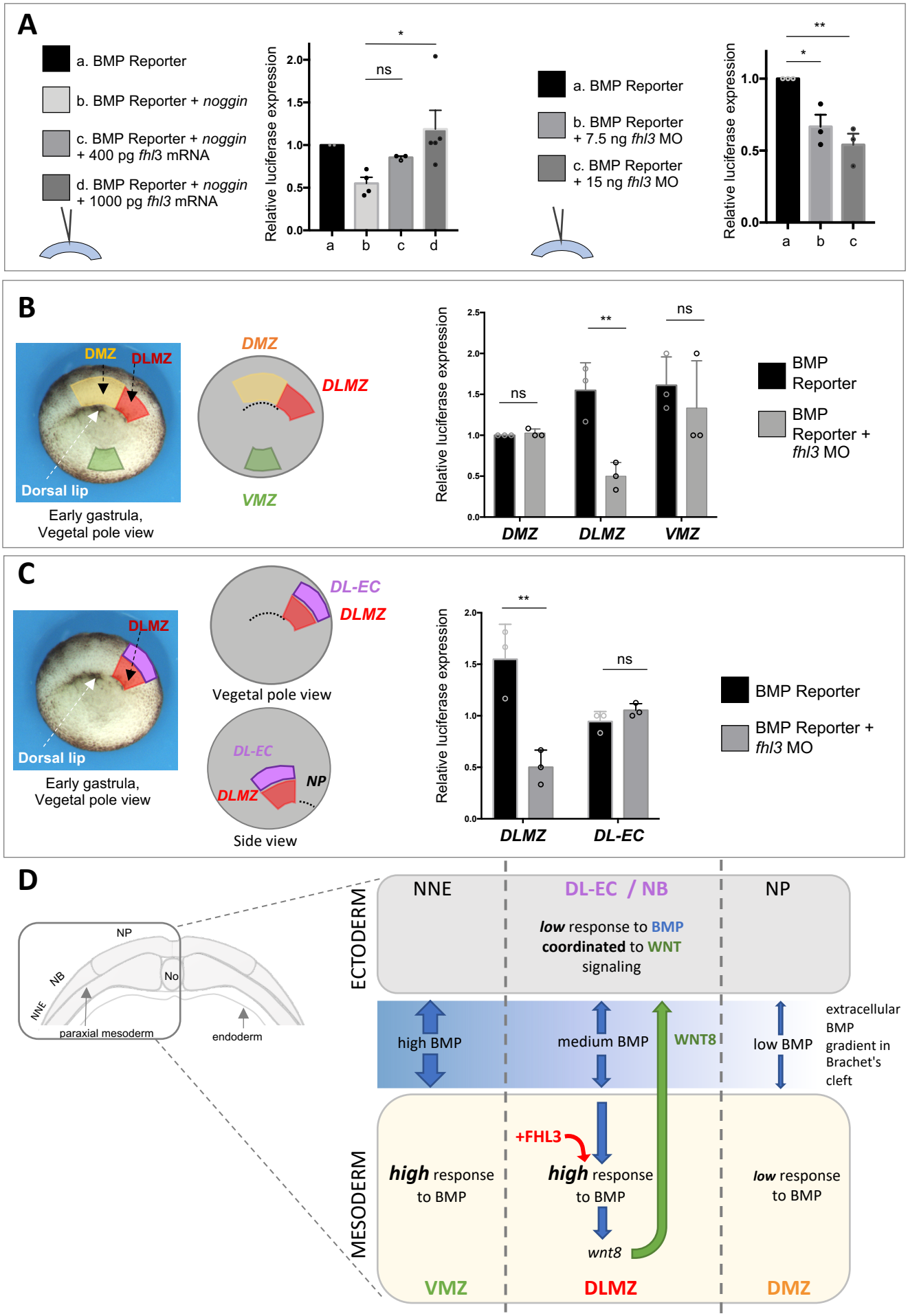
A
a. BMP Reporter
b. BMP Reporter + noggin
c. BMP Reporter + noggin + 400 pg fhl3 mRNA
d. BMP Reporter + noggin + 1000 pg fhl3 mRNA
Relative luciferase expression
ns
*
a b c d
a. BMP Reporter
b. BMP Reporter + 7.5 ng fhl3 MO
c. BMP Reporter + 15 ng fhl3 MO
**
*
a b c
B
DMZ
DLMZ
Dorsal lip
Early gastrula, Vegetal pole view
VMZ
ns
**
DMZ DLMZ VMZ
BMP Reporter
BMP Reporter + fhl3 MO
C
DL-EC
Vegetal pole view
Side view
NP
Early gastrula, Vegetal pole view
DLMZ DL-EC
D
NP
NB
No
NNE
paraxial mesoderm
endoderm
ECTODERM
NNE
DL-EC / NB
NP
low response to BMP coordinated to WNT signaling
high BMP
medium BMP
WNT8
low BMP
extracellular BMP gradient in Brachet's cleft
MESODERM
+FHL3
high response to BMP
wnt8
low response to BMP
VMZ
DLMZ
DMZ

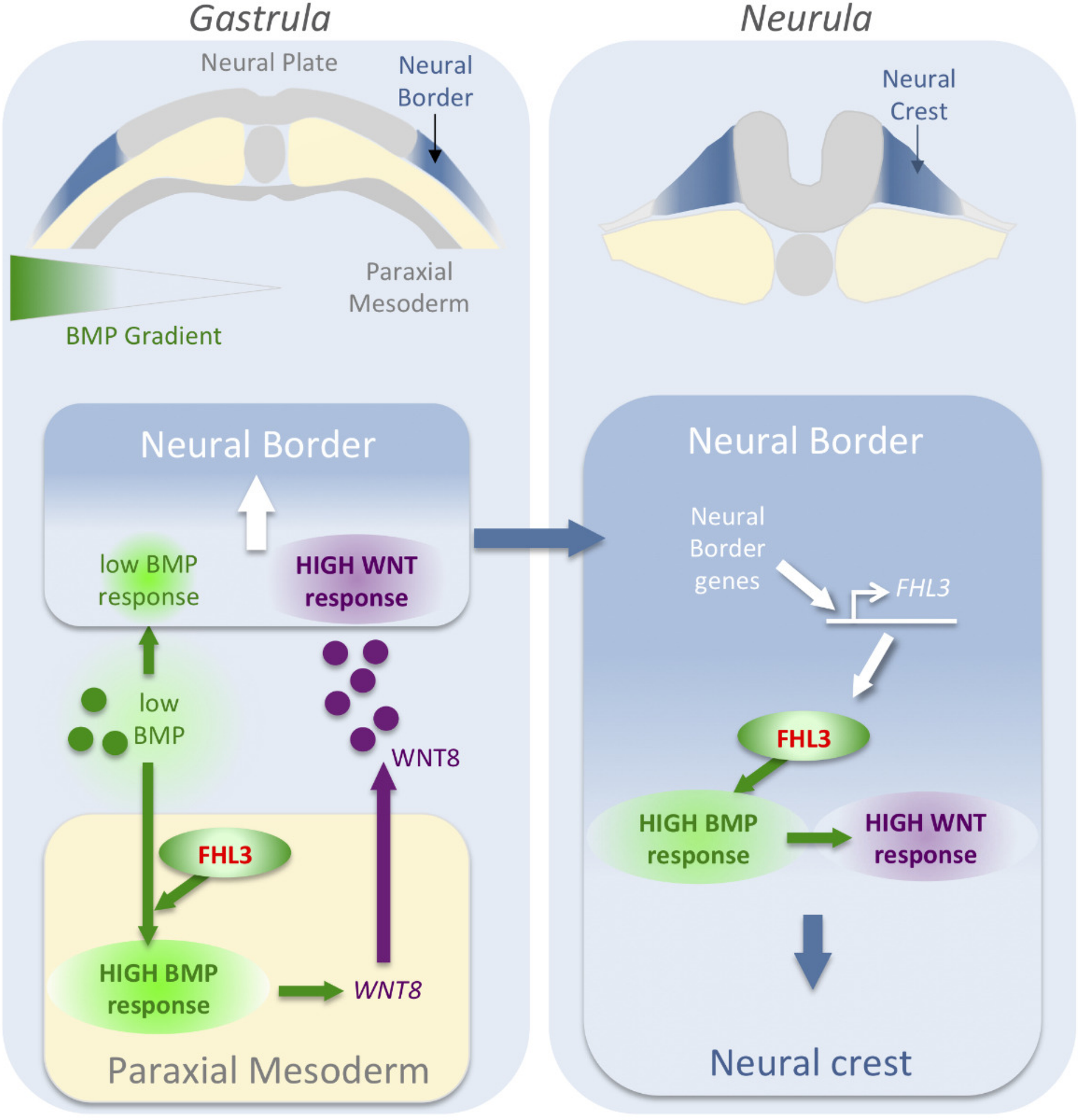
Gastrula
Neurula
Neural Plate
Neural Border
Neural Crest
Paraxial Mesoderm
BMP Gradient
Neural Border
low BMP response
HIGH WNT response
low BMP
WNT8
FHL3
HIGH BMP response
WNT8
Paraxial Mesoderm
Neural Border
Neural Border genes
FHL3
FHL3
HIGH BMP response
HIGH WNT response
Neural crest